Oncogene (2012) 31, 3148–3163

www.nature.com/onc

ORIGINAL ARTICLE

SASP mediates chemoresistance and tumor-initiating-activity of mesothelioma cells

C Canino[1], F Mori[2], A Cambria[3], A Diamantini[4], S Germoni[5], G Alessandrini[6], G Borsellino[4], R Galati[2], L Battistini[4], R Blandino[3], F Facciolo[6], G Citro[5], S Strano[2], P Muti[7], G Blandino[1] and M Cioce[1]

[1]Translational Oncogenomic Unit, Italian National Cancer Institute 'Regina Elena', Rome, Italy; [2]Molecular Chemoprevention Group, Italian National Cancer Institute 'Regina Elena', Rome, Italy; [3]S Vincenzo Hospital, Taormina, Italy; [4]Neuroimmunology Unit IRCCS Santa Lucia Foundation, Rome, Italy; [5]SAFU Department, Italian National Cancer Institute 'Regina Elena', Rome, Italy; [6]Unit of Thoracic Surgery, Italian National Cancer Institute, Rome, Italy and [7]Scientific Director's Office, Italian National Cancer Institute 'Regina Elena', Rome, Italy

Here we show that pemetrexed-treated mesothelioma cells undergo accelerated senescence. This is characterized by the secretion of proinflammatory and mitogenic cytokines, reminiscent of an SASP (senescence-associated secretory phenotype). Conditioned media from senescent MPM (malignant pleural mesothelioma) cells trigger the emergence of EMT (epithelial-to-mesenchymal)-like, clonogenic and chemoresistant cell subpopulations, expressing high levels of ALDH (aldehyde dehydrogenase) activity (ALDH^{bright} cells). We show by fluorescence-activated cell sorting of purified ALDH^{bright} and ALDH^{low} cells, that both cell-autonomous and cell-non-autonomous mechanisms converge to maintain the SASP-induced, EMT-like cell subpopulations. Chemoresistant ALDH^{bright} cells exist within primary MPM specimens and enrichment for ALDH^{bright} cells correlates with an earlier tumor onset into NOD/SCID mice. We show that RAS^{v12} expression induces SASP-like changes in untransformed human mesothelial cells, and that p53 ablation increases the effect of RAS^{v12} expression. We identify STAT3 activation as a crucial event downstream to SASP signaling. In fact, small hairpin RNA-mediated ablation of STAT3 deeply attenuates the induction of EMT genes and the increase of ALDH^{bright} cells induced by SASP-cytokines. This strongly affects the chemoresistance of MPM cells *in vitro* and leads to anticancer effects *in vivo*.
Oncogene (2012) **31,** 3148–3163; doi:10.1038/onc.2011.485; published online 24 October 2011

Keywords: EMT; chemoresistance; SASP; mesothelioma

Introduction

In addition to its role in tumor suppression, cellular senescence is increasingly recognized as an active program of cell stress response characterized by distinct epigenetic and metabolic changes and by broad effector mechanisms, such as DNA damage response (Campisi, 2001; Ben-Porath and Weinberg, 2004). In addition, genotoxic stress and oncogene expression promote a complex senescence leading to the secretion of cytokines and pro-mitogenic factors, named SASP (senescence-associated secretory phenotype; Rodier *et al*., 2005; Young and Narita, 2009; Coppe *et al*., 2010; Laberge *et al*., 2011). SASP-induced chemokines are known to induce EMT (epithelial-to-mesenchymal)-like changes in neighboring cell populations, and this may be considered as a mechanism of tumor progression (Laberge *et al*., 2011). However, it is not entirely clear whether SASP signaling can impinge on the progression of the neoplastic disease by modulating chemoresistance and tumor-initiating-activity. Here we aim to investigate this by using malignant pleural mesothelioma (MPM) as an experimental model. MPM can be an appropriate model for this study for several reasons. First, MPM is characterized by an extraordinary resistance to commonly used chemotherapeutic agents, such as pemetrexed and cisplatin, whose administration increases survival of patients of only few months (Hazarika *et al*., 2005). Indeed, a large fraction of short-term primary cultures from mesothelioma patients exhibits intermediate-to-extreme drug resistance *in vitro* (Mujoomdar *et al*., 2010). Second, recent evidence show that upregulation of senescence markers in MPM patients undergone platinum-based therapy is associated with a worse prognosis (Sidi *et al*., 2011). Third, SASP-induced cytokines are known to be autocrine and paracrine growth- and invasion-promoting signaling molecules for malignant mesothelioma *in vitro* and *in vivo* (Fujino *et al*., 1996; Galffy *et al*., 1999; Albonici *et al*., 2009; Hillegass *et al*., 2010). In the present work, we show that both pemetrexed treatment and RAS^{v12} expression trigger SASP-like changes in transformed and untransformed mesothelial cells. This stimulates the emergence of chemoresistant cell subpopulations with features of mesenchymal, tumor-initiating cells. We show that both cell-autonomous and cell-non-autonomous mechanisms maintain the SASP-induced EMT-like cell subpopula-

Correspondence: Dr G Blandino or Dr M Cioce, Translational Oncogenomic Unit, Regina Elena Cancer Institute, via Elio Chianesi 53, Rome 00144, Italy.
E-mails: blandino@ifo.it or mcioce@ifo.it
Received 23 May 2011; revised and accepted 18 September 2011; published online 24 October 2011

tions. Chemoresistant ALDH (aldehyde dehydrogenase)^{bright} cells exist within primary MPM specimens, and enrichment for ALDH^{bright} cells correlates with an earlier tumor onset in NOD/SCID mice. Finally, we identify STAT3 activation as a crucial event downstream to SASP signaling. shRNA-mediated STAT3 ablation affects the number of ALDH^{bright} cells and the chemoresistance of MPM cells *in vitro* and *in vivo*.

Results

MPM cell lines contain clonogenic chemoresistant cell subpopulations

We evaluated the viability of multiple MPM cell lines (and of a primary, untransformed human mesothelial cell line, (HMC) treated with pemetrexed (0–80 μM, 72 h). We observed a dramatic drop in cell viability of HMC cells, while a significant fraction of MPM cells survived the treatment even at high doses of pemetrexed (Figure 1a). Drug-response assay performed with surviving (replated) MPM cells confirmed a relative increase of chemoresistant cells, as shown by increased CC_{50} (cytotoxic concentration, the concentration that reduces cell viability by 50%) values (Supplementary Figures 1A and B). Clonogenic assays with either short-term-treated (5–50 μM, 6-h pulse, Figure 1b, upper panel) or chronically treated MSTO211H cells (5–50 μM, 96-h pulse, Figure 1b, lower panel) revealed that prolonged treatment with pemetrexed selected for highly clonogenic cells (Figure 1b, lower panel). Interestingly, pemetrexed treatment (10 μM, 96 h) concomitantly triggered cell senescence in a significant fraction of the MPM cells (60%), as assessed by the positivity of the treated cells for senescence-associated β-galactosidase (SA-β-Gal) staining (Figures 1c and d, left), by the drop in 5′-bromo-2′-deoxyuridine (BrdU) incorporation (Figure 1d, middle) and by the increased levels of p21 mRNA (Figure 1d, right).

Senescent MPM cells secrete cytokines and pro-mitogenic factors

The coexistence of both senescent and clonogenic cells within the pemetrexed-treated MPM cells suggest that paracrine factors produced by senescent MPM cells could modulate the behavior of the neighboring cell subpopulations, according to a SASP model (Coppe *et al*., 2010). Quantitative PCR (Q–PCR) revealed that pemetrexed (and not vehicle)-treated MSTO211H cells showed upregulation of IL6, IL8, VEGF-A and of IFNγ, CXCL1 and PlGF1 mRNAs (Figure 1e), which paired with the increased secretion of the mentioned factors in the conditioned medium (CM) (Figure 1f). This response was a feature of other pemetrexed-treated MPM cell lines (Supplementary Figure 2A).

CM derived from senescent MPM cells triggers EMT features in vitro *and* in vivo

We tested the effect of CM from pemetrexed-treated (p-CM), senescent MSTO211H cells on their untreated counterparts (as compared with CM from vehicle-treated cells (v-CM)). We found that p-CM (and not v-CM) treated cells acquired a scattered, elongated fibroblast-like morphology, reminiscent of a mesenchymal phenotype (Figure 2a, left vs right panels). Notably, no or little induction of cell senescence was observed in the p-CM-treated cell populations (Figure 2b). Next, we found that p-CM treated cells were strongly vimentin-positive (Figure 2c left vs right panel) and showed an increased migratory capacity (Figure 2d, left and right panels). QRT–PCR revealed high levels of ICAM1 and fibronectin mRNAs (Figure 2e), and a significant increase of vimentin, MMP-9 and of two EMT-effectors, such as SNAIL and SLUG (Figure 2e). All of the upregulated genes have been associated with the acquisition of EMT and invasive properties in solid malignancies (Ruco *et al*., 1996; Scarpa *et al*., 2002; Sivertsen *et al*., 2006; Schramm *et al*., 2010; Casarsa *et al*., 2011). p-CM treatment of other MPM cell lines triggered similar changes (Supplementary Figure 2B). Next, to test whether the p-CM-induced effects contributed to the acquisition of tumorigenic properties *in vivo*, we performed xenograft transplantation assays (Figure 2f). Analysis of the clinical signs of the xenografted mice revealed that mice transplanted with p-CM-pretreated MSTO211H and NCI-H2052 cells (1 week before transplantation) showed a higher frequency and reduced latency of tumor development (Supplementary Figures 2C and D). This significantly affected mice survival (66.6% vs 16.7% residual survival for v-CM and p-CM-treated MSTO211H cells, and 100% vs 33% residual survival for v-CM and p-CM- treated NCI-H2052 cells at day 115, respectively, $P<0.05$, Figure 2f). These observations pair with the results of the *in vitro* clonogenic assays (Figure 1b, lower panel).

p-CM-induced MPM cell subpopulations are enriched for ALDH^{bright} cells

In many solid tumors, the expression of high levels of ALDH has been associated to the presence of tumorigenic, invasive and chemoresistant cell subpopulations (Adhikari *et al*., 2011). Interestingly, fluorescence-activated cell sorting (FACS) analysis revealed that the EMT-like, p-CM- (and not v-CM) selected cell subpopulations were highly enriched for ALDH^{bright} cells (Figure 3a). Notably, treatment with p-CM strongly increased the number of ALDH^{bright} cells in all the analyzed MPM cell lines (Supplementary Figure 3A). This suggests that soluble factors in the medium of the pemetrexed-treated cells can modulate the number of ALDH^{bright} cells. Indeed, FACS analysis revealed that some of the cytokines identified in the p-CM increased the number of ALDH^{bright} cells, with PlGF1, IL8, VEGF and IFNγ being the most effective in this regard (Figure 3b). We also observed a degree of crosstalk between the identified factors: for example, IL8, VEGF and IFNγ treatment increased the levels of PlGF1mRNA (Supplementary Figure 3B) indicating that p-CM contains cytokines acting as a complex network.

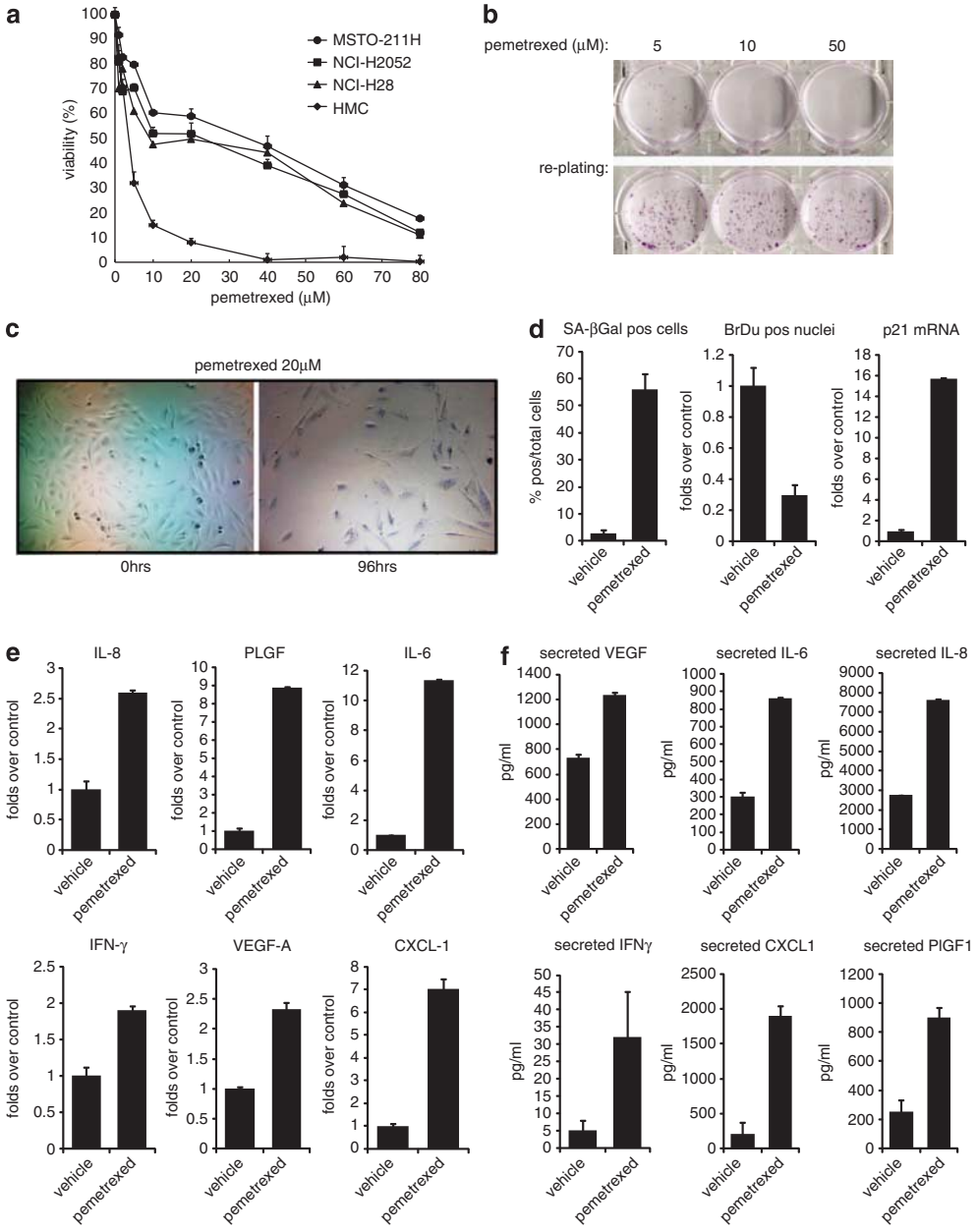

Figure 1 MPM cell lines undergo accelerated senescence upon pemetrexed treatment. (**a**) Dose–curve response of 3 MPM cell lines and of a normal mesothelial cell line (HMC) to pemetrexed treatment (72 h). (**b**) CFA assay: Representative micrographs of colonies formed by MSTO211H cells treated with pemetrexed as indicated for 6 h (upper panel) or 96 h (lower panel) before seeding. (**c**) SA-β-Gal staining of MSTO211H cells treated with pemetrexed (20 μM) for the indicated times. (**d**) Histograms showing the number of SA-β-Gal-positive cells (right), of BrdU-positive nuclei (middle) and p21 mRNA levels (left) of cells treated as from C. (**e**) Q–PCR for the expression of the indicated proinflammatory and mitogenic cytokines from either vehicle- and pemetrexed-treated cells (20 μM, 96 h). (**f**) ELISA quantification of secreted cytokines from cells treated as in (**e**). Bars indicate the average of three independent experiments. Statistics: $P<0.05$.

MPM ALDH^{bright} cells exhibit TIC properties

To characterize the ALDH^{bright} cell subpopulation induced by p-CM, we FACS-sorted to purify ALDH^{bright} cells and ALDH^{low} cells from MSTO211H cells, and evaluated their response to pemetrexed treatment (Figures 3c and d). This showed that purified ALDH^{bright} cells were highly resistant to pemetrexed treatment (Figure 3c) and highly clonogenic (Figure 3d), as compared with ALDH^{low} cells. Migration assays revealed that ALDH^{bright} cells were capable to invade matrigel much more efficiently than ALDH^{low} cells (Figure 4e, left panel). *In situ* ALDH assay confirmed that most of the migrated cells were ALDH^{bright} cells (Figure 4e, right panel). This finding is relevant as we found that purified ALDH^{bright} cells rapidly divide by generating both ALDH^{low} and ALDH^{bright} cells, whereas purified ALDH^{low} cells do not generate ALDH^{bright} cells (Supplementary Figure 4). Q–PCR analysis of freshly

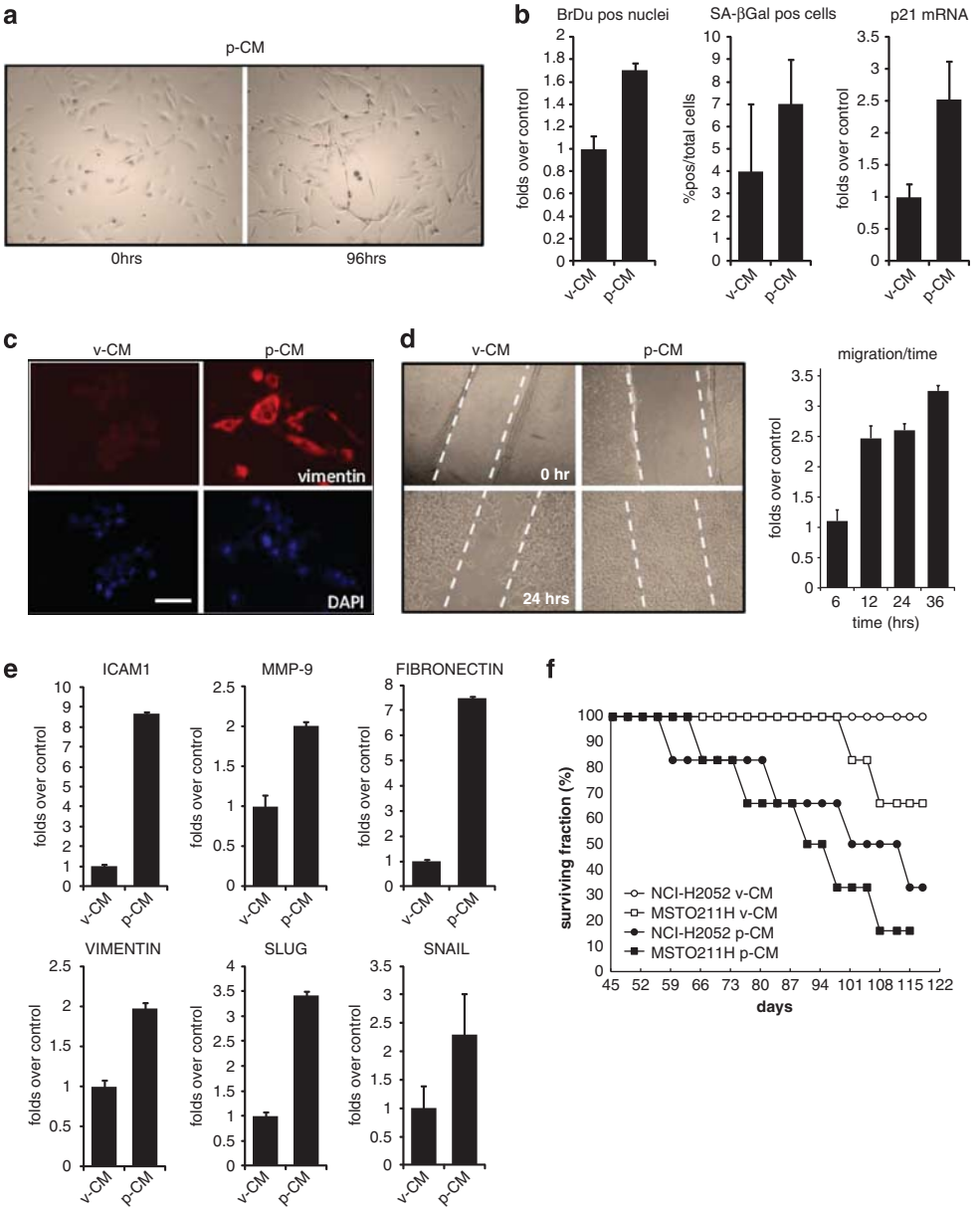

Figure 2 CM from pemetrexed-treated MPM cells triggers EMT features. (**a**) Representative micrographs of MPM cells treated with CM from pemetrexed-treated cells at the indicated times. (**b**) Histograms showing the number of SA-β-Gal-positive cells (right), of BrdU-positive nuclei (middle) and p21 mRNA levels (left) of cells treated as from (**a**). (**c**) Indirect immunofluorescence of MSTO211H cells treated for 24 h with p-CM or v-CM. Red: vimentin. blue: DAPI staining. Scale bar: 100 μM. (**d**) Left panel: Representative wound-healing closure assays of MSTO211H cells treated with p-CM or v-CM for 24 h. Right panel: Histogram showing the healing closure efficiency of MSTO211H cells treated as from left panel at the indicated times. (**e**) Q–PCR for the expression of the indicated EMT genes from cells treated as indicated for 24 h. Bars indicate the average of three independent experiments. Statistics: $P<0.05$. (**f**) Survival curve of CD1 mice xenografted with MSTO211H and NCI-H2052 cells pre-treated with v-CM or p-CM. $n=6$. Statistics: $P<0.05$.

purified MPM ALDH^{bright} cells revealed higher mRNA levels of MMP9 and of other two EMT factors, such as SNAIL and SLUG (Figure 3f), which correlated with the higher invasive ability of ALDH^{bright} cells. We also found very high mRNA levels of ABCG2, Nanog, Oct4, Musashi and Sox2, with Nanog, Sox2 and OCT4 being upregulated >70-folds in ALDH^{bright} cells (Figure 3g). Expression of the latter genes is associated with a poorly differentiated, tumorigenic cell phenotype in many solid malignancies (refer Discussion). Therefore, p-CM-induced ALDH^{bright} cells show both EMT-like and TIC features.

Cell-autonomous signaling fuels expansion of ALDH^{bright} cells within pemetrexed-treated MPM cells

Next, we evaluated in greater detail the effect of pemetrexed on purified ALDH^{bright} cells (Figure 4). This showed that ALDH^{bright} cells undergo senescence to a

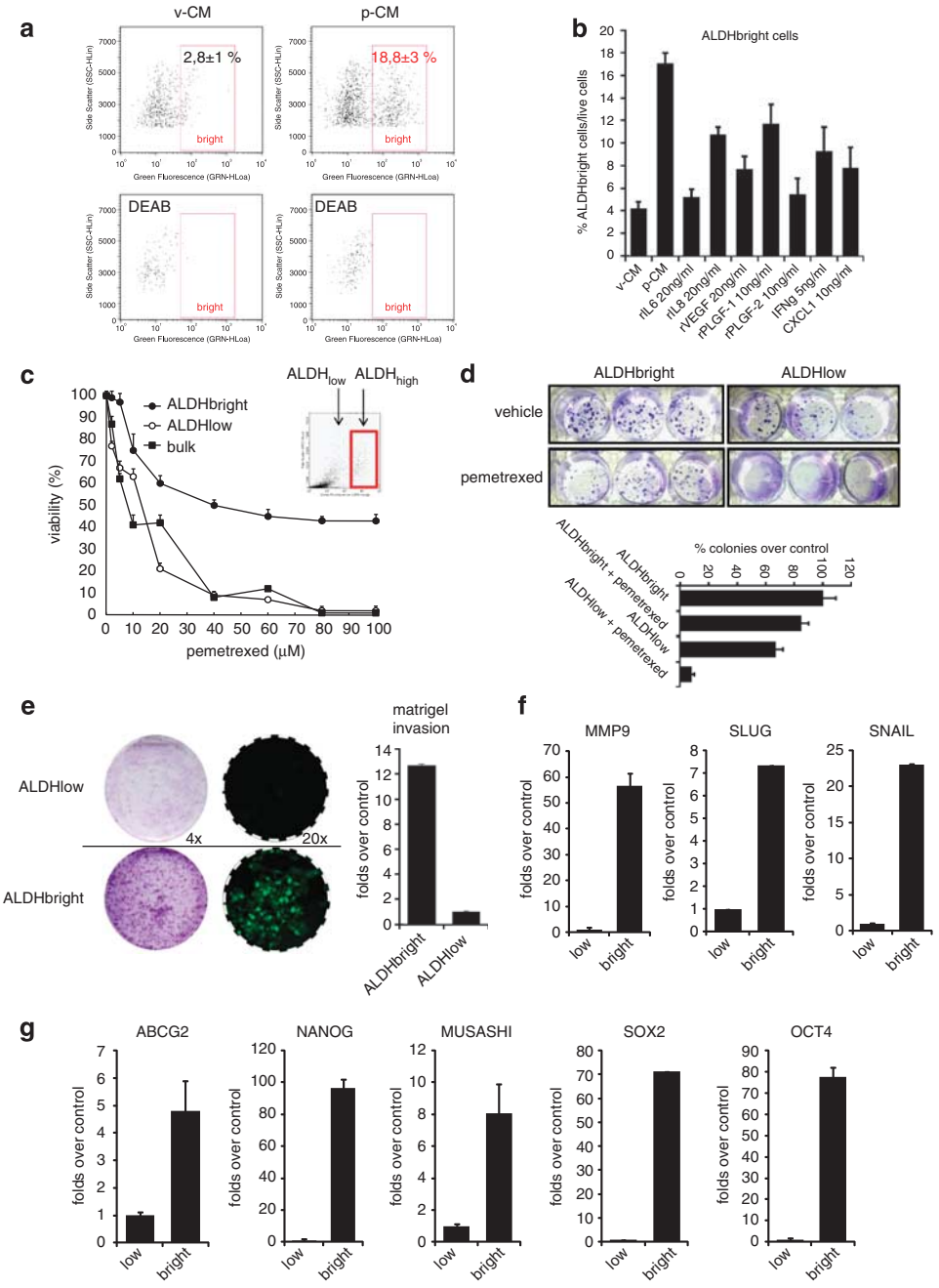

Figure 3 p-CM-induced cell subpopulations are enriched for clonogenic, chemoresistant ALDH^{bright} cells. (**a**) Upper panels: Representative FACS plots showing the percentage of ALDH^{bright} cells from MSTO211H cells treated as indicated. Lower panels: Negative control obtained by treating cells with DEAB, an irreversible inhibitor of the ALDH activity. (**b**) Histograms showing the percentage of ALDH^{bright} cells from MSTO211H cells treated with the indicated cytokines for 48 h. Bars indicate the average of three independent experiments. (**c**, **g**) Purified ALDH^{bright} cells possess TIC features. (**c**) Dose–response curves of FACS-sorted ALDH^{low}, ALDH^{bright} and bulk (unsorted) MSTO211H cells to pemetrexed treatment. The inset shows the scheme used for FACS-based sorting of ALDH^{bright} and ALDH^{low} cells. (**d**) Clonogenic assay. Upper panel: Representative micrographs of CFA assays with sorted ALDH^{bright} and ALDH^{low} cells treated with either vehicle or pemetrexed (50 μM, 6 h) and seeded at 100 cells per well in a six-well dish. Lower panel: Histograms showing average colony counts from triplicate experiments. (**e**) Matrigel invasion assay. Left: Crystal violet staining of matrigel-migrated ALDH^{bright} and ALDH^{low} cells. Right: *In situ* ALDH activity assay of migrated cells as from the left panel. (**f**, **g**) QRT-PCR: Fold changes in mRNA expression levels of the indicated TIC/EMT genes of FACS-sorted ALDH^{bright} relative to ALDH^{low} MSTO211H cell subpopulations. Error bars represent mean ± s.d. v-CM: conditioned medium from vehicle-treated cells; p-CM: conditioned medium from pemetrexed-treated cells. Error bars represent mean ± s.d.

much lesser extent than ALDH^{low} cells (26 ± 4% vs 85 ± 1.3 %, respectively, as revealed by SA-β-Gal staining, Figure 4a). This was accompanied by a concomitant increase in the number of ALDH^{bright} cells (Figure 4b), which did not take place for purified ALDH^{low} cells. Interestingly, analysis of the cytokines

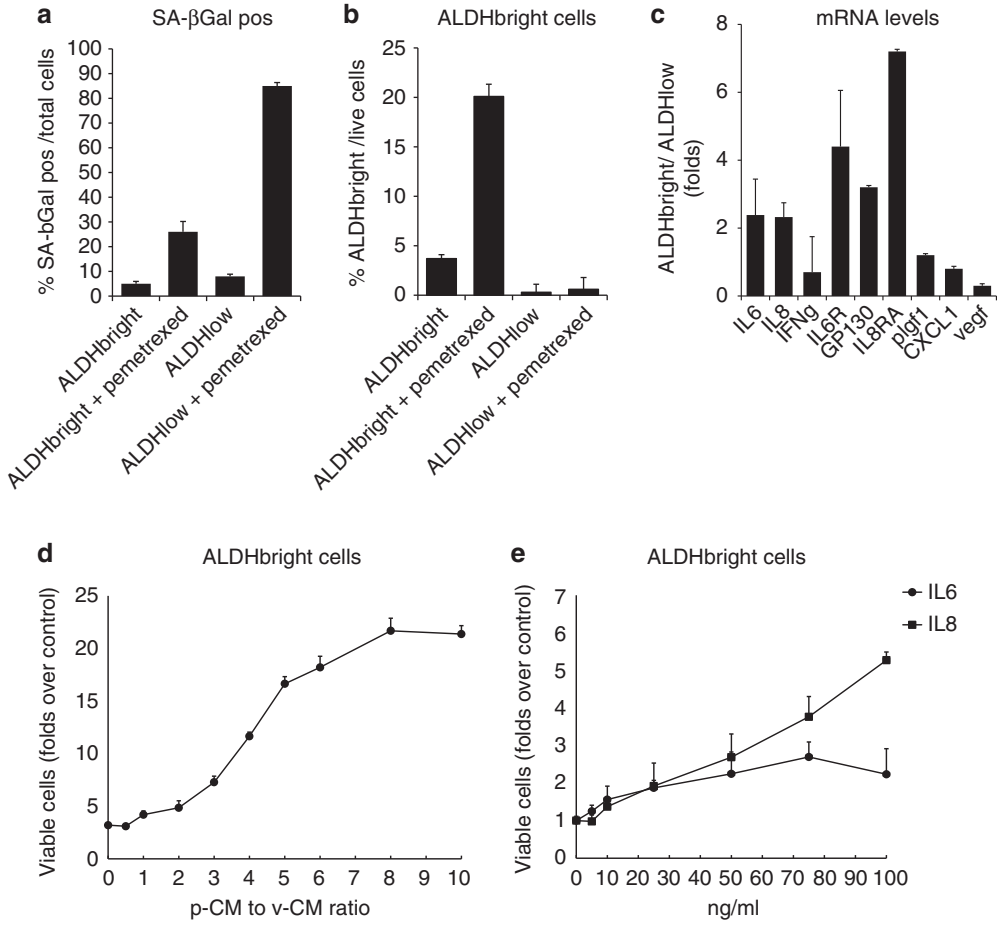

Figure 4 (**a**) SA-β-Galstaining of MSTO211H ALDH^{bright} and ALDH^{low} cells treated with pemetrexed (20 μM, 96 h). (**b**) FACS-based evaluation of ALDH^{bright} cell number of purified cells treated as from (**a**). (**c**) Q–PCR mRNA expression levels of the indicated cytokine and cytokine receptors expressed as a ratio of mRNA levels between ALDH^{bright} and ALDH^{low} cells. (**d**, **e**) Dose–response curves of freshly sorted ALDH^{bright} cells to p-CM (**d**) and to recombinant IL6 and IL8 (**e**). Y-axis indicates the number of ALDH^{bright} cells evaluated by FACS. Error bars represent mean ± s.d.

expressed by pemetrexed-treated ALDH^{bright} vs ALDH^{low} cells revealed that the ALDH^{bright} cells were endowed with higher levels of IL6, IL8, and of IL6R, IL8R and Gp130 mRNAs (Figure 4c). In line with this, we found that treatment of naive ALDH^{bright} from MSTO211H cells with CM from ALDH^{bright}-treated cells increased dose-dependently the number of ALDH^{bright} cells (Figure 4d), and that rIL6 and rIL8 had similar growth-promoting effects (Figure 4e). This suggests that the increase in ALDH^{bright} cell number induced by pemetrexed treatment of MPM cells may be mediated by IL6 and IL8 produced in a cell-autonomous manner.

ALDH^{bright} cells exist in vivo *and survive pemetrexed treatment*

To assess whether the observed SASP-induced ALDH^{bright} cell subpopulations exist within primary samples, we derived primary cells by mechanical and enzymatic disaggregation of freshly excised human surgical specimens (meso nos. 1, 2 and 4) or from pleural effusions (meso nos. 3 and 5–9). FACS analysis showed that a variable percentage of ALDH^{bright} cells could be readily identified in 9 out of 9 samples (Supplementary Figure 5). We found that 9/9 MPM primary cell cultures survived chronical pemetrexed treatment (2 weeks–10 μM every 72 h) and 8/9 showed a time-dependent increase of ALDH^{bright} cells (Figure 5a), together with a concomitant increase of SA-β-Gal-positive cells (Figure 5b). Soft-agar CFA assays revealed that chronically selected primary cultures were more clonogenic than those exposed to vehicle alone (Figure 5c, inset).

SASP modulates MPM development in primary MPM xenografts

We then investigated whether the increase of ALDH^{bright} cells in MPM primary cultures correlates with their tumorigenicity *in vivo*. Quasi-orthotopic transplantation assays with two primary cultures (meso nos. 4 and 5) revealed that NOD/SCID mice transplanted with pemetrexed-selected cells developed peritoneal mesothelioma with higher efficiency (3/6 for meso no. 4 and 6/6 for meso no. 5 and at day 81 post-injection (p.i.),

respectively, Figure 5d) as compared with those transplanted with vehicle-treated cells (0/6 for meso no. 4 and 1/6 for meso no. 5 at day 81 p.i., respectively, Figure 5d). Morphological analysis (H/E (hematoxylin and eosin) and staining for human calretinin) of the formalin-fixed excised lesions confirmed the human nature of the material and the diagnosis of malignant mesothelioma in all cases (Figure 5e). Notably, FACS analysis of the excised tumors (when available) revealed that the lesions generated by chronically treated MPMs were significantly enriched for ALDH^{bright} cells ($13.5 \pm 2\%$ vs $35 \pm 5\%$ for meso no. 5 vs meso no. 5-pemetrexed tumors, respectively, Figure 5d). Moreover, we found that mRNA levels of ICAM1, Fibronectin, Vimentin, as well as those of Oct4, Nanog and ABCG2 were higher in the more aggressive tumors (Figure 5f upper and lower panel). We also found that intratumoral mRNA levels and the quantity of secreted IL8, PLGF and VEGF-A into the peritoneal lavage fluid of mice were significantly increased in mice transplanted

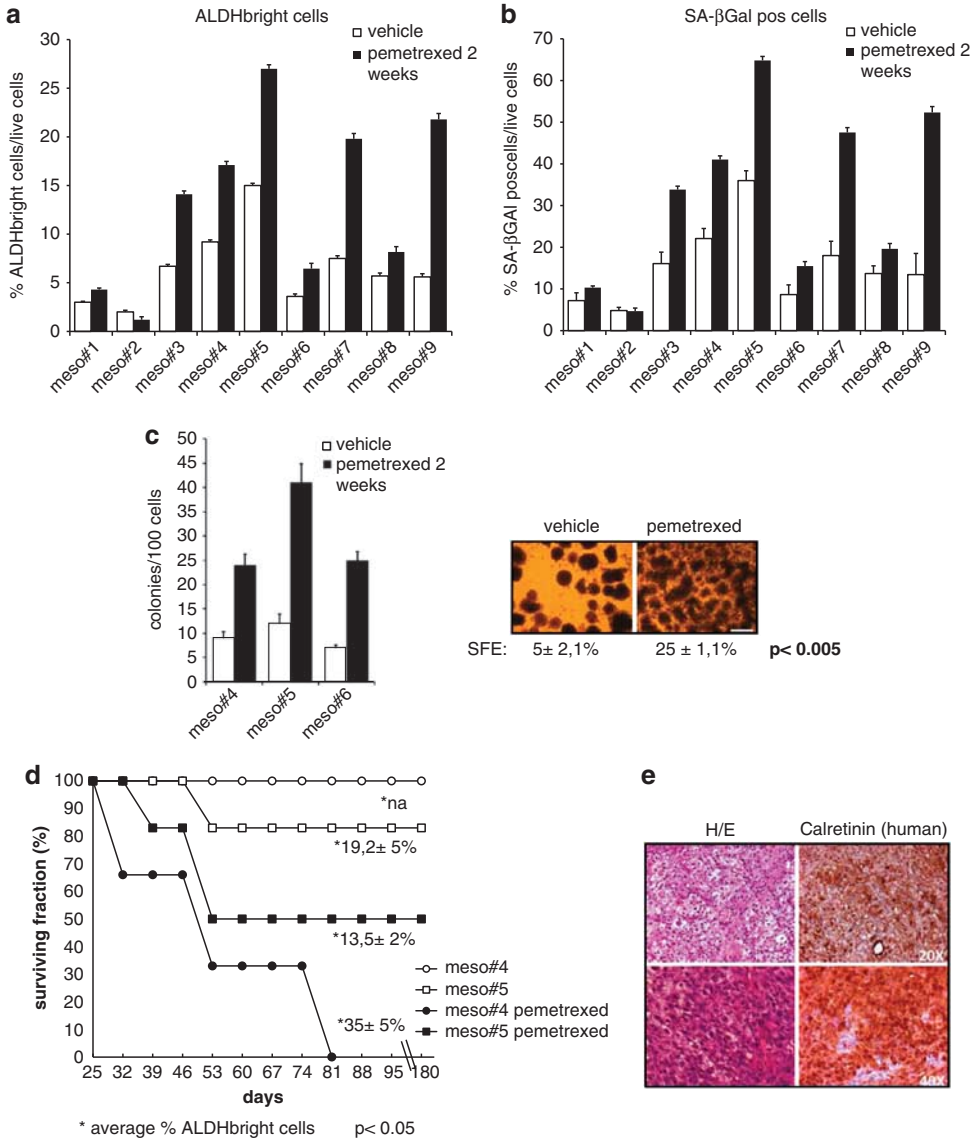

Figure 5 Chemoresistant ALDH^{bright} cells exist *in vivo*. Histogram showing the percentage of ALDH^{bright} cells (**a**) and the percentage of SA-β-Gal-positive cells (**b**) in primary MPM cultures treated with vehicle or pemetrexed as indicated. (**c**) Left: Histogram showing the average colony counts from primary MPM cultures treated as from (**a**, **b**). An average of three independent experiments is reported. Right: Representative micrographs of the formed colonies from cells treated as from (**a**, **b**). Scale bar: 100 μm. (**d**) Enrichment for ALDH^{bright} cells affects MPM engrafment in NOD/SCID mice. Quasi-orthotopicxenograft transplantation experiments ($n = 6$) with two representative primary MPM cultures (no. 4 and no. 5) chronically treated with either vehicle- or pemetrexed as from (**a**). Survival curves: Asterisks indicate the number of ALDH^{bright} cells within pooled tumors/each group at day 81 p.i. Statistics: $P < 0.05$. (**e**) H/E staining and anti-(human) calretinin expression of representative sections of engrafted mesotheliomas as from (**d**). (**f**) Q–PCR. Fold changes in mRNA expression levels of the indicated senescence/TIC/EMT genes from tumors collected from the indicated xenografted mice. (**g**) mRNA levels (upper panel) and ELISA quantification of secreted human cytokines (lower panel) from peritoneal washings of the indicated xenografted mice. Bars indicate the average of three independent experiments. Error bars represent mean ± s.d.

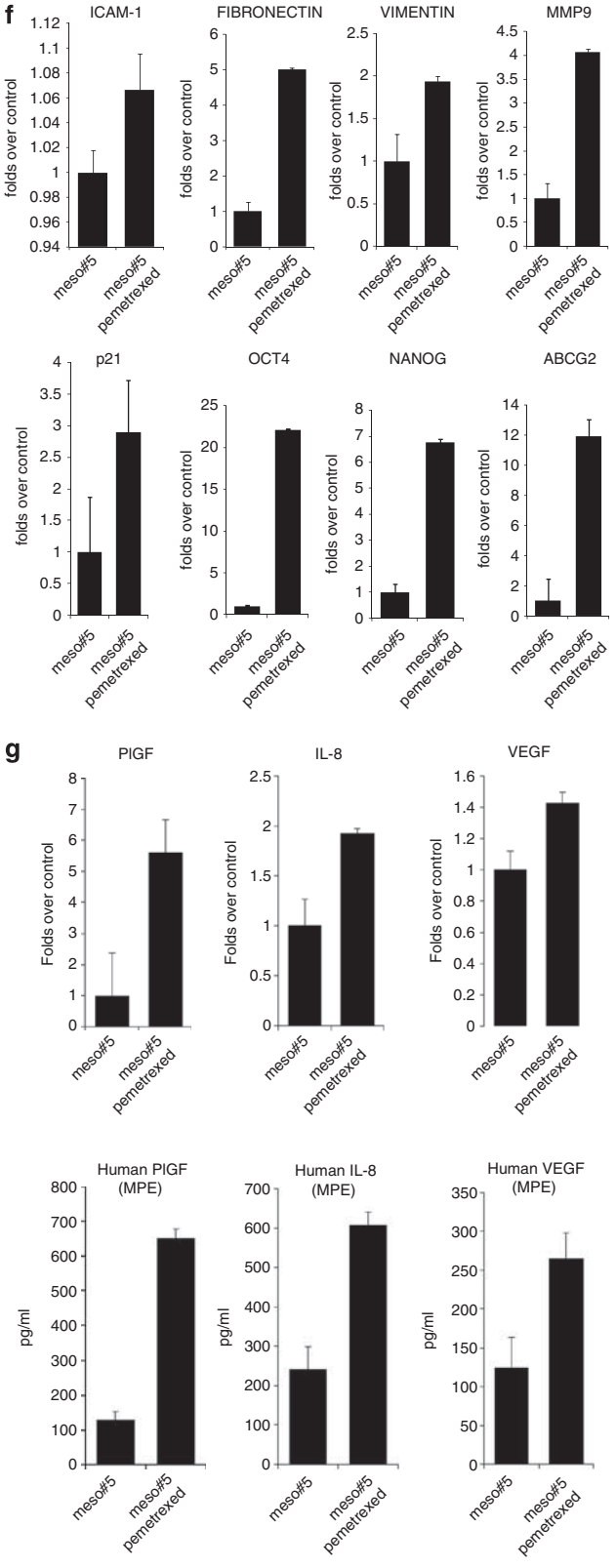

Figure 5 Continued.

with the more aggressive tumors (Figure 5g, upper and lower panels). Altogether, these findings suggest that many of the changes induced by p-CM in MPM cell lines (Figures 1–3) occur in xenografted primary MPMs as well.

RAS^{V12}–induced SASP modulates MPM ALDH^{bright} cell number

Expression of oncogenic RAS has been shown to induce a strong SASP in untransformed fibroblasts, and this appears to be restrained by the p53 pathway (Coppe *et al*., 2008). Therefore, to widen our observations regarding the pemetrexed-induced SASP in MPM cells, we tested whether expression of oncogenic RAS induces similar changes into HMC cells, and whether alteration of the p53 pathway could enhance the effect of RAS^{v12}. In order to do this, we first evaluated the status of p53 in the HMC and MPM cell lines in our collection (Supplementary Figure 6) Direct sequencing of p53 exons 5–8 showed that almost all of the cell lines are endowed with wtp53 alleles, except for MMP-89 cells that bear a deletion of both chromosomes 17 (Supplementary Figure 6A). Moreover, cisplatin treatment increased p53 levels and triggered nuclear accumulation of p53 of representative cell lines (Supplementary Figures 6B and C). Next, we retrovirally transduced HMC cells with either control- or RAS^{V12}-expressing vectors (pBABE and pBABE-RAS^{v12}, respectively) and 5 days later we performed RNA interference with either scrambled- or p53-targeting small hairpin RNAs (shRNAs) (Figure 6). We found that RAS^{V12} expression induced the appearance of flat, enlarged SA-β-Gal-positive cells in both scrambled- and shP53- transfected cells within 8 days p.i. (Figures 6a and b). This paired with a strong induction of IL6, IL8, IFNγ and CXCL1 mRNAs, which were higher in RAS^{v12}-shP53 HMC cells (Figure 6c). CM from both RAS^{V12}/scrambled cells and RAS^{v12}/shp53 HMC cells strongly increased the number of ALDH^{bright} cells (Figure 6d), and the mRNA levels of both EMT (SLUG, SNAIL and MMP9) and CSC (Oct4 and Nanog) markers (Figure 6e) on naive HMC cells. We reproducibly observed a more marked effect of the medium from RAS^{v12}/shp53 HMC cells (Figures 6c–e), suggestive of an increased SASP. This suggests that oncogenic RAS expression induces SASP-like changes in MPM cells reminiscent of those elicited by pemetrexed treatment.

STAT3 signaling is required for the SASP-induced chemoresistance in vivo *and* in vitro

Some of the cytokines we identified in the p-CM or induced by RAS^{v12} expression are known to activate STAT3 signaling (such as IL6 and IFNγ) or to be STAT3 target genes (such as VEGF, PLGF and IL8). In line with this, we found that p-CM treatment of both HMC and MPM cells induced a significant increase of STAT3 (Y^{705}) phosphorylation in absence of changes in the STAT3 protein levels (Figure 7a). In addition, p-CM treatment promoted an increased nuclear accumulation of p-STAT3 (Y^{705}) (Figure 7b). To assess the relevance of STAT3 phosphorylation for the p-CM-induced effects, we generated MPM cell lines stably knocked down for STAT3 (Figure 7c). We found that STAT3

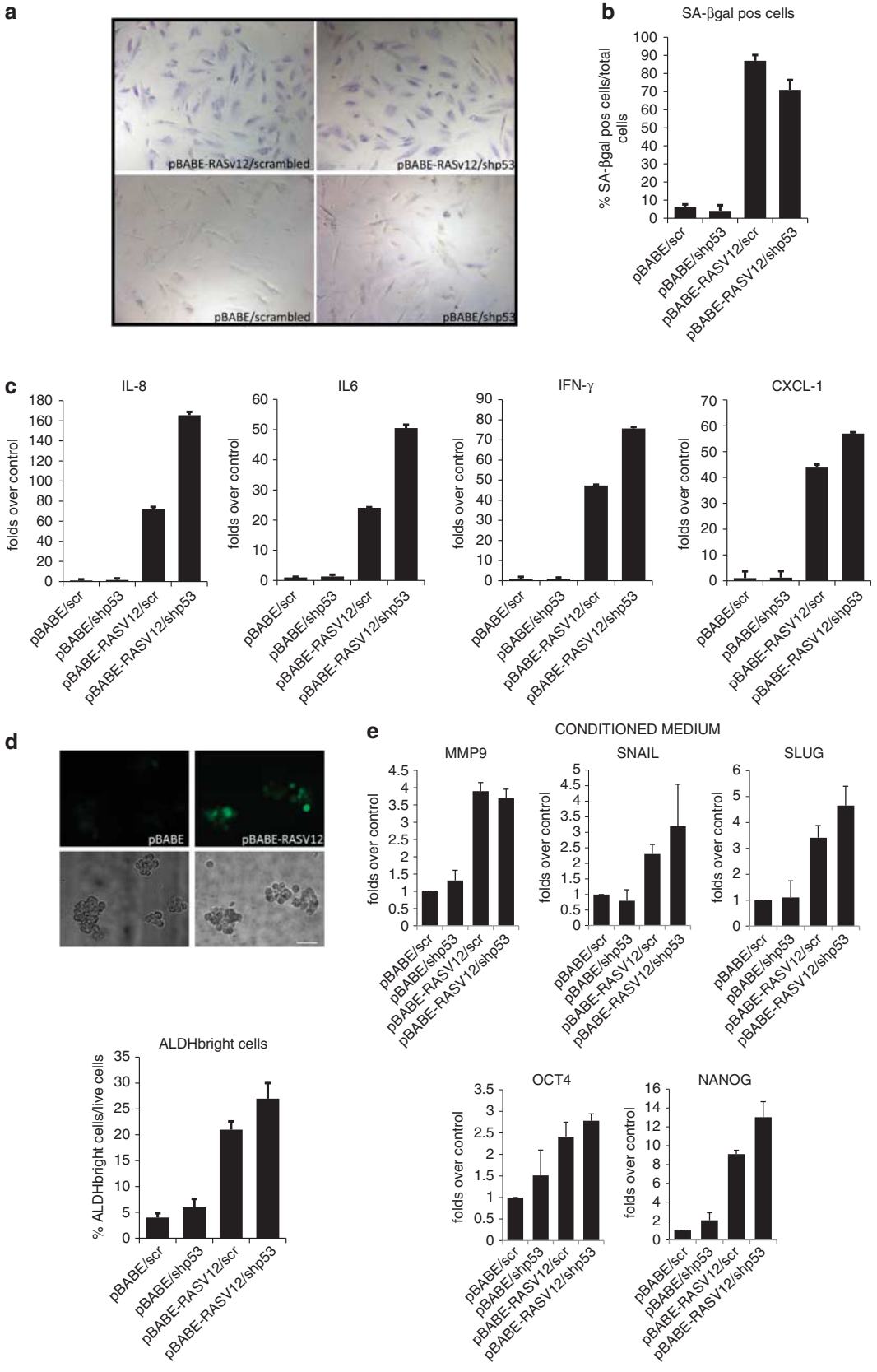
a
pBABE-RASv12/scrambled
pBABE-RASv12/shp53
pBABE/scrambled
pBABE/shp53
b
SA-βgal pos cells
% SA-βgal pos cells/total cells
pBABE/scr
pBABE/shp53
pBABE-RASV12/scr
pBABE-RASV12/shp53
c
IL-8
IL6
IFN-γ
CXCL-1
folds over control
d
pBABE
pBABE-RASV12
ALDHbright cells
% ALDHbright cells/live cells
e
CONDITIONED MEDIUM
MMP9
SNAIL
SLUG
OCT4
NANOG

knockdown strongly affected the resistance of MSTO211H and NCI-H2052 to pemetrexed treatment, as revealed by both viability and clonogenic assays (as compared with cells transduced with scrambled shRNA, Figures 7d and e, respectively). Moreover, we found that the number of ALDH^{bright} cells in the STAT3 k/d cells was deeply reduced both in basal conditions (v-CM) and upon p-CM treatment (Figure 7f). Finally, we found that induction of some EMT genes by p-CM was strongly reduced as well (Figure 7g). To investigate whether STAT3 activation has a role in mediating SASP-induced effects *in vivo*, we performed xenograft assays with either scrambled- or -STAT3 k/d MSTO211H (scrambled and shSTAT3, respectively). We started pemetrexed treatment (i.p injection every 3 days at 100 mg/kg, Figure 7h, arrows) when the engrafted tumors were $\geqslant 0.1\,cm^3$ in volume (day 1, Figure 7h). First, we observed that among the vehicle-treated mice, the tumors formed by STAT3 k/d cells were smaller as compared with the ones formed by control cells (Figure 7h). In addition, we found that all the engrafted tumors were sensitive to pemetrexed treatment (Figure 7h), with the tumors from STAT3 k/d cells being the most sensitive ones. Indeed, a prolonged inhibition of tumor growth was observed in mice carrying STAT3 k/d tumors and treated with the antifolate (Figure 7h, $P<0.05$). We obtained similar results with STAT3 k/d NCI-H2052 cells (data not shown). Interestingly, FACS analysis of representative excised tumors ($n=4$) revealed that the tumors formed by STAT3 k/d cells were endowed with much lower number of ALDH^{bright} cells, thus pairing our *in vitro* observations (Figure 7f).

Discussion

The work presented on this paper investigates mesothelioma chemoresistance, a major feature of MPM, which strongly influences the history of the disease. We show here, for the first time, that pemetrexed treatment of mesothelioma cell lines and primary MPM cells readily induces a senescent phenotype with features of SASP (Coppe *et al*., 2010) (Figure 1). SASP consists of premature senescence and secretion of a complex mix of cytokines, chemokines and growth factors (Laberge *et al*., 2011). We show that treatment of naive MPM cells with CM derived from pemetrexed-treated MPM cells promotes the emergence of mesenchymal-like, chemoresistant cell subpopulations endowed with high levels of ALDH activity (ALDH^{bright} cells). ALDH^{bright} cells are a minor fraction of unfractionated MPM cell populations. However, purified ALDH^{bright} cells (as compared with ALDH^{low} cells) show prominent tumorigenic properties *in vitro,* and their number correlates with frequency and latency of mesothelioma development in NOD/SCID mice (Figures 2 and 5). In addition, purified ALDH^{bright} cells rapidly generate ALDH^{low} cells and reconstitute the composition of the originating culture, according to a 'progenitor-like' status (Supplementary Figure 4). ALDH^{low} cells, in turn, produce cytokines that promote expansion of ALDH^{bright} cells (Figures 3b and 4c). Therefore, both ALDH^{low} and ALDH^{bright} cell subpopulations may closely cooperate in determining the transformed MPM phenotype through cell-autonomous as well as non-autonomous mechanisms (Figure 8, model). EMT-like cells with high ALDH activity and tumorigenic features have been described in many solid and non-solid tumors (Charafe-Jauffret *et al*., 2010; Cioce *et al*., 2010; Kryczek *et al*., 2011; Ma and Allan, 2011; Marcato *et al*., 2011; Wang *et al*., 2011). In addition, it has been recently shown that the expansion of breast ALDH^{bright} cells is sustained by mesenchymal bone marrow-derived cells. This is mediated by IL-8 (Liu *et al*., 2011). Mesothelial cells acquire mesenchymal features in response to a variety of inflammatory conditions (Park *et al*., 2003; Aroeira *et al*., 2007; Kim *et al*., 2011). It is tempting to speculate whether mesothelial cells may functionally substitute the bone marrow-derived cells described by Liu *et al*. (2011) during the inflammation-driven progression of MPM. This is the first time, to our knowledge, that a direct link between SASP and chemoresistance has been addressed. Interestingly, this is significant in regards to the inverse relationship between expression of senescence markers and patient survival observed by Sidi *et al*. (2011) in chemo-treated primary MPMs. Thus, the presence of senescent MPM cells within growing tumours seems to be required for tumour survival. Our *in vivo* studies do not demonstrate that ALDH^{bright} cells are responsible for MPM development. However, the pro-tumorigenic behaviour demonstrated by ALDH^{bright} cells *in vitro* and *in vivo* calls for future studies to be conducted on a larger cohort of patients. An increase of ALDH^{bright} cells (for example, in the pleural exudate of patients) could be of diagnostic or prognostic value in staging MPM.

We attempted to explain SASP-mediated signaling in pemetrexed-treated cells in more detail. We identified STAT3 activation as a crucial event downstream to SASP-induced cytokine signaling in MPM cells. STAT3 is a possible prerequisite for the modulation of EMT genes by SASP-induced cytokines, and is important to maintain the ALDH^{bright} cell pool (Figure 7). In fact, shRNA-mediated depletion of STAT3 potentiates the effect of pemetrexed *in vivo* (Figure 7). The relevance of STAT3 signaling for MPM cells is reinforced by the observation that most SASP cytokines identified here are either STAT3 activators (IL6 and IFNγ) or known

Figure 6 RAS^{v12} expression induces SASP and increases MPM ALDH^{bright} cell number. (**a**) SA-β-Gal staining of HMC cells retrovirally transduced with the indicated expression vectors. (**b**) Histograms showing the number of SA-β-Gal-positive cells as from (**a**). (**c**) QRT–PCR. mRNAlevels of the indicated proinflammatory and mitogenic cytokines from cells transduced as indicated. (**d**) Upper panel: *In situ* ALDH assay of HMC cells trasduced as indicated. Lower panel: FACS-based analysis of ALDH^{bright} cells in HMC cells as from A. (**e**) QRT–PCR. Fold changes in mRNA expression levels of the indicated TIC/EMT genes of naive HMC cells treated with CM from the indicated cells. Bars indicate the average of three independent experiments.

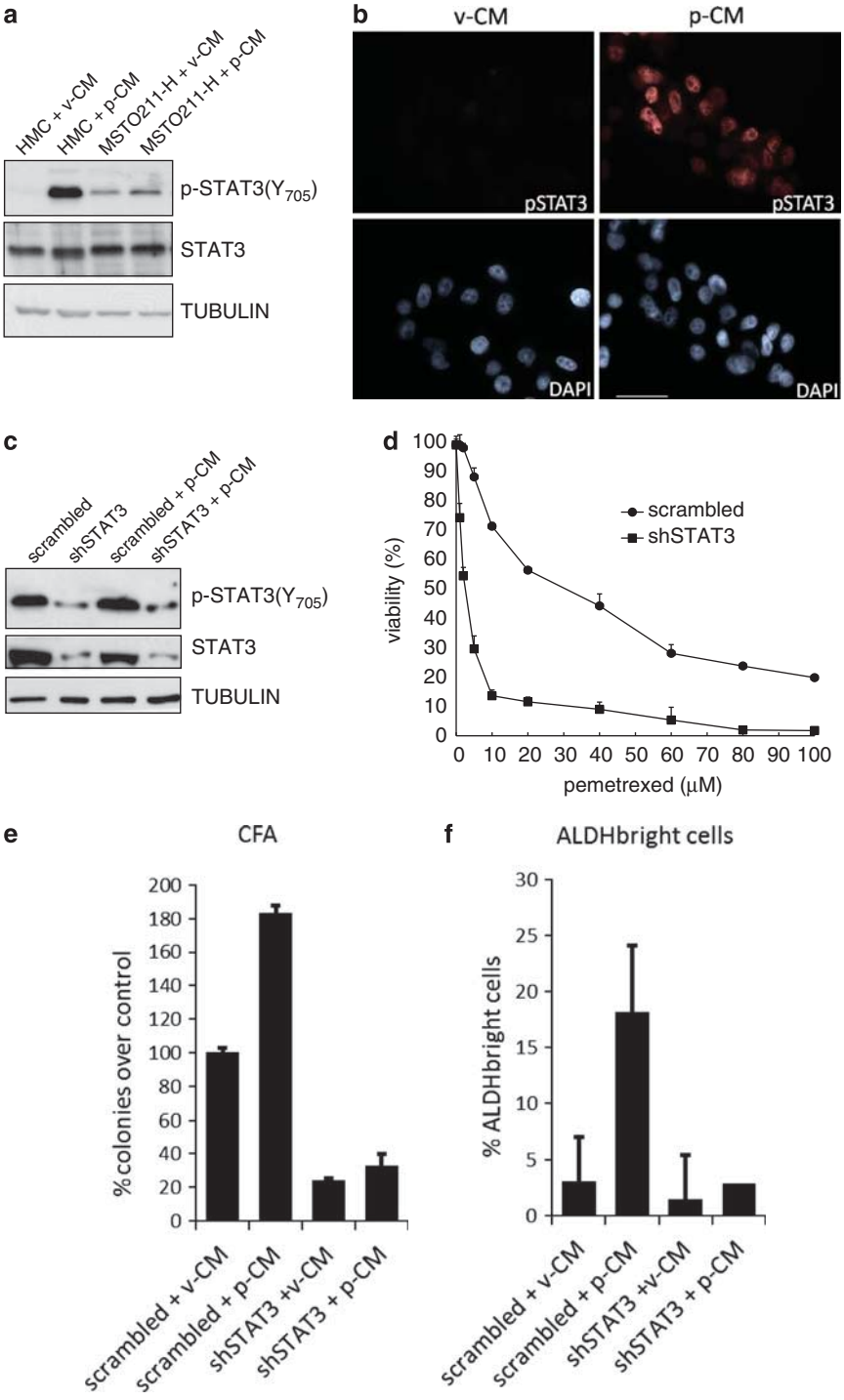

Figure 7 STAT3 is required for SASP-induced chemoresistance *in vivo* and *in vitro*. (**a**) Representative western blot analysis of whole cell lysates obtained from HMC and MSTO211H cells treated with p-CM for 30 min. Upper panel: Anti-pSTAT3 (Y^{705}) staining. Middle panel: anti-STAT3 antibody. Lower panel: Loading control (anti-tubulin staining). (**b**) Indirect immunofluorescence of MSTO211H cells treated for 30 min with p-CM or v-CM. Red: pSTAT3 (y^{705}). Blue: DAPI staining. Scale bar: 30 μm. (**c**) Representative western blot analysis of whole cell lysates obtained from MSTO211H cells transduced with either scrambled- or STAT3-shRNA-targeting vectors and treated with p-CM for 30 min. Upper panel: Anti p-STAT3 (Y^{705}) staining. Middle panel: Anti-STAT3 antibody. Lower panel: Loading control (anti-tubulin staining). (**d**) Dose–response curves of MSTO211H cells as from C to pemetrexed treatment. (**e**) Histograms showing average colony counts of scrambled- and shSTAT3 MSTO211H cells treated with v-CM and p-CM. (**f**) Histogram showing the percentage of $ALDH^{bright}$ cells in scrambled- and shSTAT3-transduced MSTO211H cells treated as from 7E. (**g**) Q–PCR. Fold changes in mRNA expression levels of the indicated EMT genes from scrambled- and shSTAT3-transduced MSTO211H cells treated as indicated. Error bars represent mean ± s.d. (**h**) Tumor volume of xenografted tumors from scrambled- and shSTAT3-transduced MSTO211H cells treated i.p. with pemetrexed (100 mg/kg per 3 days, $n = 4$) when the tumor volume was $\geqslant 0.1\,cm^3$. $P < 0.05$; asterisks (*) indicate no statistically significant differences between the samples. (**i**) Histograms showing the percentage of $ALDH^{bright}$ cells from representative excised tumors ($n = 4$) as from 5H. Statistics: $P < 0.05$.

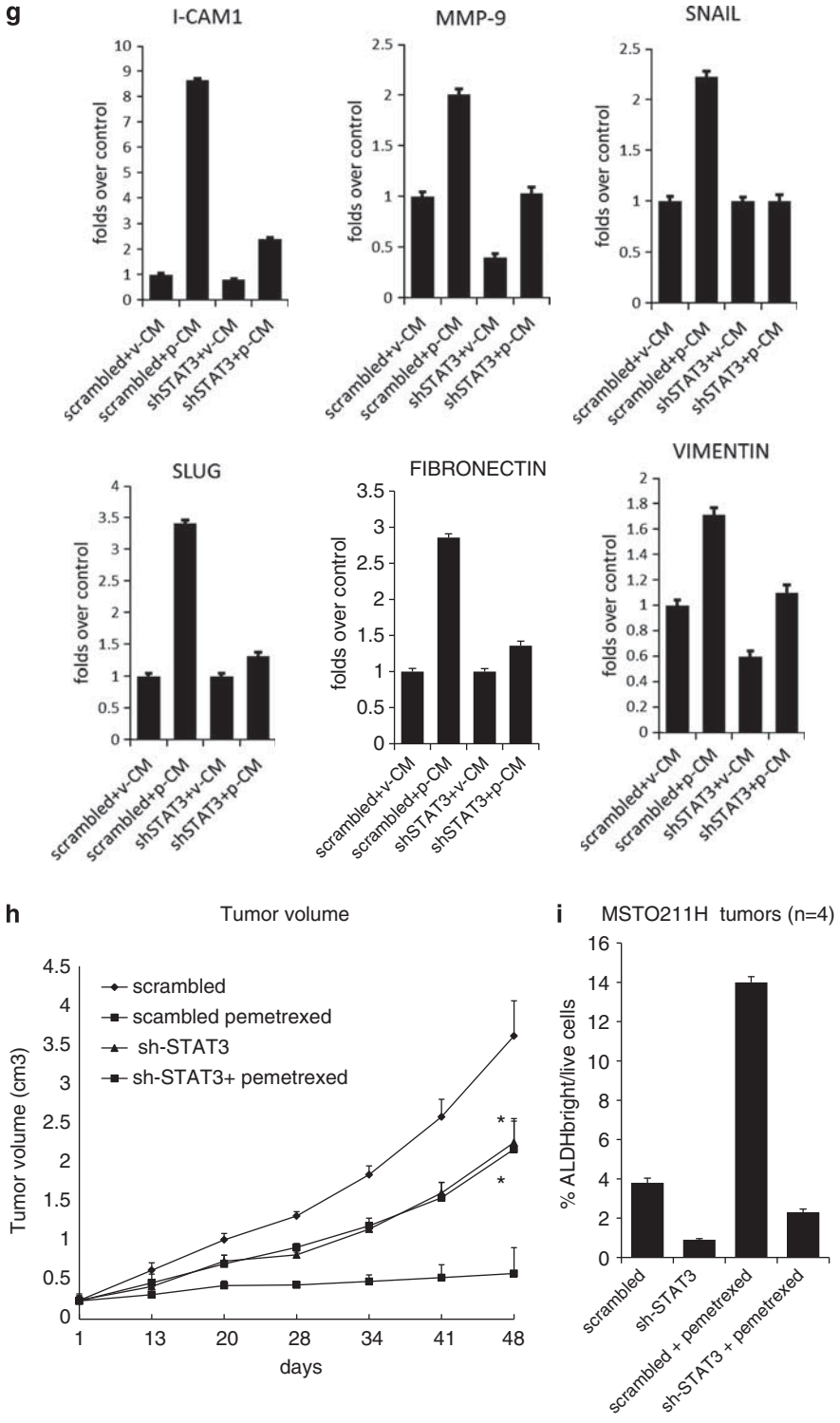

Figure 7 Continued.

STAT3 target genes (IL8, PLGF and VEGF) (Takeda and Akira, 2000; Schindler *et al*., 2007; Oka *et al*., 2010; Huang *et al*., 2011a,b). Notably, some of them are prognostically relevant for MPM *in vivo*, such as PLGF1 (Albonici *et al*., 2009; Pompeo *et al*., 2009). Additionally, nuclear positivity for pSTAT3 has been described in 60% of malignant mesothelioma cases (Achcar Rde *et al*., 2007).

Our data suggest that the involvement of p53 pathway in MPM, typically considered as a wtp53-carrying tumor (Metcalf *et al*., 1992; Mor *et al*., 1997), must be further investigated. We show that RNAi-mediated

downregulation of p53 strongly affects the magnitude of SASP in HMC cells infected with RAS^{v12} (Figure 6). Despite our data being obtained by artificially manipulating the levels of p53 in wtP53-HMC and -MPM cells (Supplementary Figure 6), evidence that downstream p53 signaling may be altered in MPM is accumulating. It is worthy to note that downregulation of mir-34 b/c (by promoter methylation) in MPM cells has been recently described by Kubo *et al*. (2011). Mir-34b/c are direct transcriptional targets of p53 and part of the p53 tumor suppressor network (He *et al*., 2007; Hermeking, 2007). In addition, some of the deregulated targets of mir-34 b/c may be involved in SASP signaling, such as c-Met (Corney *et al*., 2007), which is the HGF ligand. The MET/HGF axis is frequently altered in MPM (Tolnay *et al*., 1998). We suggest that the strong tendency of mesothelial cells undergoing EMT upon inflammatory stimuli (such as asbestos exposure) and functional alterations of the p53 pathway (with consequent deregulation of possible SASP effectors) may favor the emergence of SASP-induced chemoresistant cell subpopulations in MPM. We observed that SASP-induced tumorigenic properties (EMT, chemoresistance, acquisition of migratory/invasive properties and progenitor-like features) appear to be mediated by distinct sets of cytokines with partially overlapping functions. This may explain the limited therapeutic efficacy of single cytokine-targeting agents in MPM observed to date (Li *et al*., 2007; Bais *et al*., 2010; Suzuki *et al*., 2010; Yao *et al*., 2011). Therefore, we believe that interference with STAT3 signaling (a broad modulator of SASP-induced effects) may be a promising strategy in counteracting MPM chemoresistance.

Materials and methods

Cell lines and culture conditions
The human MPM cell lines MSTO211H, NCI-H28, NCI-H2052 and NCI-H2452 were obtained from the ATCC (Rockville, MD, USA). MPP-89 cells were obtained from the Istituto Nazionale per la Ricerca sul Cancro, Genova, Italy. HMC cells were from Tebu-Bio, Le Perray en Yvelines, France. All the cell lines were cultured as monolayers at 37 °C and 5% CO_2 in DMEM/F12 + GLUTAMAX (Invitrogen-Gibco, Carlsbad, CA, USA) supplemented with 10% non-heat inactivated FBS (fetal bovine serum) (Invitrogen-Gibco) and 5 μg/ml insulin (Sigma-Aldrich, St Louis, MO, USA). Before treatment with CM or recombinant cytokines, cells were shortly (6 h) cultured in starvation medium DMEM/F12 + GLUTAMAX supplemented with 1% BSA-FAF (fatty acid-free bovine serum albumin) and 5 μg/ml insulin (Sigma-Aldrich).

Primary MPM cultures
Primary MPM cultures (meso nos 1, 2 and 4) were generated as follows: briefly, solid tissues were manually minced and subjected to collagenase/ialuronidase digestion (300U/100U, respectively) for 2 h in digestion medium (DMEM/F12 + GLUTAMAX supplemented with 1% BSA-FAF and 5 μg/ml insulin). Digested material was then filtered through a nylon mesh (70 μm), collected by gentle centrifugation and resuspended in fresh medium DMEM/F12 + GLUTAMAX (1:1, Invitrogen, Carlsbad, CA, USA) supplemented with 5% non-heat inactivated FBS, insulin 10 μg/ml and ciprofloxacin (4 μg/ml). Pleural effusions (meso nos 3, 5 and 9) were centrifuged for 10 min at 1000 r.p.m. before being treated as primary MPMs.

ALDH activity assay and cell sorting
ALDH activity was detected *in situ* by using a fluorescence microscope or by FACS analysis (Guava easyCyte, Millipore, Billerica, MA, USA). ALDEFLUOR kit (Stem Cell Technologies, Vancouver, Canada) was used in both cases, according to the manufacturer's instructions. Sorting of MPM cell subpopulations was performed by using a MoFlo FACS instrument (DAKOCytomation, Carpinteria, CA, USA) equipped with a refrigerated chamber. ALDH-positive cells were defined as the cells that displayed greater fluorescence compared with a control staining reaction containing the ALDH inhibitor, DEAB (diethylaminobenzaldehyde).

Cell viability assay
Cell viability of treated cells was assessed by ATPlite assay (Perkin Elmer, Boston, MA, USA) according to manufacturer's instructions.

Reagents and cytokines
Pemetrexed (Eli Lilly and Company, Indianapolis, IN, USA), Cisplatin (Sigma-Aldrich), IL6 and IL8 (ORF Genetics, Kopavogur, Iceland); VEGF (BD Biosciences Pharmingen, San Diego, CA, USA); PLGF1 (ProspectBio, Rehovot, Israel); IFNγ (Millipore, Billerica, MA, USA) and CXCL1 (R&D, Minneapolis, MN, USA) were all dissolved according to manufacturer's instructions.

SA-β-Gal staining
SA-β-galactosidase staining was performed on adherent cells according to published protocols (Debacq-Chainiaux *et al*., 2009).

Cytokine quantification
Levels of secreted IL6, IL8, IFNγ and VEGF from CM or peritoneal washing fluid of mice were quantitated by Human Singleplex Bead Kit (Invitrogen). Quantikine Immunoassay (R&D) was used to quantify CXCL1 and PlGF1 levels, respectively.

BrdU incorporation assay
Detection of BrdU incorporation was performed by ELISA (BrdU Cell Proliferation Assay Kit, Cell Signaling Technology, Danvers, MA, USA) according to the manufacturer's instructions.

Wound healing assay
Cells grown to 95% confluence were seeded in 6-well tissue culture plates and wounded with a sterile 10-μl pipette tip to remove cells. Digital micrographs were taken after scratching and at the indicated times.

Invasion assay
Matrigel invasion assays were performed as follows: Briefly, 20 μg per well of Matrigel (BD Biosciences) were applied to 24-well transwell plates with 8 μ pore size (BD Biosciences) and allowed to solidify overnight. 30 000 cells resuspended in fresh medium were seeded into each well. The plates were incubated at 37 °C for 72 h, and then cells at the bottom were fixed and stained. Transmigrated cells were normalized for initial number of seeded live cells or subjected to *in situ* ALDH assay, as indicated before.

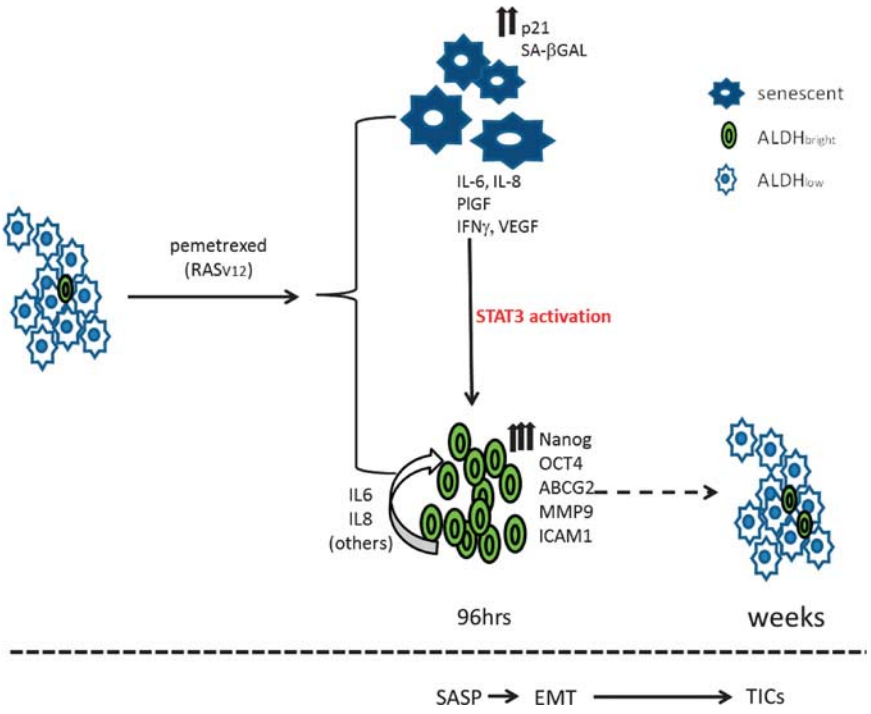

Figure 8 Schematic working model. SASP triggers EMT and TIC features in MPM by cell-autonomous and cell-non-autonomous mechanisms.

Clonogenic assay
MPM cells were seeded at 100 ($ALDH^{bright}$)-5000 (bulk) cells per 6-well dish. Formed colonies were stained with crystal violet 10–15 days later. When indicated, cells were resuspended in 0.3% methylcellulose before plating.

Q–PCR
Total RNA was extracted using the Trizol Reagent (Gibco). The first-strand cDNA was synthesized according to manufacturer's instructions (M-MLV RT kit, Invitrogen). Gene expression was measured by real-time PCR using the Sybr-Green assay (Cell Signaling Technology) on a 7900HT instrument (Applied Biosystems). Q–PCR primers are reported in Supplementary Table 1.

Xenograft transplantation
Suspensions of 1×10^6 MSTO211H cells were injected i.p. (Figure 1) or s.c. (Figure 7) in PBS1X/Matrigel (BD Biosciences) into 5-weeks-old male CD1 mice (Charles River, Milan). Body weight and clinical signs of the mice were determined every 3 days, and in case of i.p. transplantation, mesothelioma development was suggested by the presence of >2 g per week variation of body weight, worsening of clinical symptoms and appearance of ascitic fluid. For s.c. transplantation, tumor volume was calculated using the formula: $V = \pi/6 \times \text{length} \times \text{width}$ (by manual caliper). Mice were treated i.p. with pemetrexed (100 mg/kg per 3 days, $n = 4$) when the tumor volume was $\geqslant 0.1\,cm^3$. All tumorigenicity assays were carried out according to the guidelines set by the Internal Ethical Committee.

MPM transplantation in NOD/SCID mice
Suspensions of 0.5×10^6 human primary MPM cultures were injected i.p. in PBS1X/Matrigel (BD Biosciences) into 5-weeks-old male NOD/SCID mice (Charles River Laboratories, Calco, LC, Italy). Body weight and clinical signs of the mice were determined as described before. Diagnosis of malignant mesothelioma was confirmed by expert pathologists (H/E and anti-human calretinin staining (Ventana Medical Systems, Oro Valley, AZ, USA) of nine representative sections of each excised lesion).

Western blot
For Western blotting, the following antibodies were used: anti-pSTAT3 (Tyr-705) (#sc-8059), anti-STAT3 (#sc-7179), anti-Tubulin (#sc-23948) (Santa Cruz Biotechnology, Santa Cruz, CA, USA), anti-p53 (DO-1, Calbiochem, San Diego, CA, USA).

Immunofluorescence microscopy
Briefly, cells were fixed/permeabilized in paraformaldehyde/methanol, aspecific binding blocked in PBS containing 1% bovine serum albumin, and labeled with anti-Vimentin antibody (VIM-13.2 Sigma, 1:100 dilution), p-STAT3 (Tyr-705) (#sc-8059) or p53 (pantropic DO-1, Calbiochem). The secondary antibody was an Alexa 488-conjugated goat anti-mouse IgG (Calbiochem). Nuclei were visualized by 4′,6-diamidino-2-phenylindole (DAPI) staining.

Retroviral transduction of HMC and MPM cells
The pBabe, pBabe-Ras^{V12}, pRETRO SUPER p53, pRETRO, pSIH1-puro-STAT3 shRNA and pSIH1-puro-scrambled-shRNA (plasmids 26596 and 26597, Addgene, Cambridge, MA, USA) constructs were transfected into the 293T packaging cells (Invitrogen) by Ca-PO_4 precipitation method. Virus-containing supernatants were used to infect MPM or HMC cells (three cycles of infection). Cells were selected by puromycin (1 μg/ml every 48 h for 1 week).

Statistical analysis

Student's *t*-test was used to assess significance of the *in vitro* data, whereas the significance of mice survival data was determined by using Kaplan-Meier analysis and Log Rank test for statistical significance. *P* values of $\leqslant 0.05$ were considered statistically significant. When indicated, asterisks indicate no statistically significant differences between the labeled samples.

Abbreviations

EMT, epithelial-to-mesenchymal–transition; MPE, mesothelial peritoneal exudate; SASP, senescence-associated-secretory-phenotype; TICs, tumor-initiating–cells.

Conflict of interest

The authors declare no conflict of interest.

Acknowledgements

We thank Ms Tania Merlino (Regina Elena Cancer Institute, Rome) for revising and proofreading the manuscript and Dr Frank Sinicrope (Rochester, MN) for the ShSTAT3 vectors available at ADDGENE (UK). We acknowledge INAIL (Italian Workers' Compensation Authority) for grant support to GB.

References

Achcar Rde O, Cagle PT, Jagirdar J. (2007). Expression of activated and latent signal transducer and activator of transcription 3 in 303 non-small cell lung carcinomas and 44 malignant mesotheliomas: possible role for chemotherapeutic intervention. *Arch Pathol Lab Med* **131**: 1350–1360.

Adhikari AS, Agarwal N, Iwakuma T. (2011). Metastatic potential of tumor-initiating cells in solid tumors. *Front Biosci* **16**: 1927–1938.

Albonici L, Doldo E, Palumbo C, Orlandi A, Bei R, Pompeo E *et al*. (2009). Placenta growth factor is a survival factor for human malignant mesothelioma cells. *Int J Immunopathol Pharmacol* **22**: 389–401.

Aroeira LS, Aguilera A, Sanchez-Tomero JA, Bajo MA, del Peso G, Jimenez-Heffernan JA *et al*. (2007). Epithelial to mesenchymal transition and peritoneal membrane failure in peritoneal dialysis patients: pathologic significance and potential therapeutic interventions. *J Am Soc Nephrol* **18**: 2004–2013.

Bais C, Wu X, Yao J, Yang S, Crawford Y, McCutcheon K *et al*. (2010). PlGF blockade does not inhibit angiogenesis during primary tumor growth. *Cell* **141**: 166–177.

Ben-Porath I, Weinberg RA. (2004). When cells get stressed: an integrative view of cellular senescence. *J Clin Invest* **113**: 8–13.

Campisi J. (2001). Cellular senescence as a tumor-suppressor mechanism. *Trends Cell Biol* **11**: S27–S31.

Casarsa C, Bassani N, Ambrogi F, Zabucchi G, Boracchi P, Biganzoli E *et al*. (2011). Epithelial-to-mesenchymal transition, cell polarity and stemness-associated features in malignant pleural mesothelioma. *Cancer Lett* **302**: 136–143.

Charafe-Jauffret E, Ginestier C, Iovino F, Tarpin C, Diebel M, Esterni B *et al*. (2010). Aldehyde dehydrogenase 1-positive cancer stem cells mediate metastasis and poor clinical outcome in inflammatory breast cancer. *Clin Cancer Res* **16**: 45–55.

Cioce M, Gherardi S, Viglietto G, Strano S, Blandino G, Muti P *et al*. (2010). Mammosphere-forming cells from breast cancer cell lines as a tool for the identification of CSC-like- and early progenitor-targeting drugs. *Cell Cycle* **9**: 2878–2887.

Coppe JP, Desprez PY, Krtolica A, Campisi J. (2010). The senescence-associated secretory phenotype: the dark side of tumor suppression. *Annu Rev Pathol* **5**: 99–118.

Coppe JP, Patil CK, Rodier F, Sun Y, Munoz DP, Goldstein J *et al*. (2008). Senescence-associated secretory phenotypes reveal cell-nonautonomous functions of oncogenic RAS and the p53 tumor suppressor. *PLoS Biol* **6**: 2853–2868.

Corney DC, Flesken-Nikitin A, Godwin AK, Wang W, Nikitin AY. (2007). MicroRNA-34b and MicroRNA-34c are targets of p53 and cooperate in control of cell proliferation and adhesion-independent growth. *Cancer Res* **67**: 8433–8438.

Debacq-Chainiaux F, Erusalimsky JD, Campisi J, Toussaint O. (2009). Protocols to detect senescence-associated beta-galactosidase (SA-betagal) activity, a biomarker of senescent cells in culture and *in vivo*. *Nat Protoc* **4**: 1798–1806.

Fujino S, Yokoyama A, Kohno N, Hiwada K. (1996). Interleukin 6 is an autocrine growth factor for normal human pleural mesothelial cells. *Am J Respir Cell Mol Biol* **14**: 508–515.

Galffy G, Mohammed KA, Dowling PA, Nasreen N, Ward MJ, Antony VB. (1999). Interleukin 8: an autocrine growth factor for malignant mesothelioma. *Cancer Res* **59**: 367–371.

Hazarika M, White Jr RM, Booth BP, Wang YC, Ham DY, Liang CY *et al*. (2005). Pemetrexed in malignant pleural mesothelioma. *Clin Cancer Res* **11**: 982–992.

He L, He X, Lim LP, de Stanchina E, Xuan Z, Liang Y *et al*. (2007). A microRNA component of the p53 tumour suppressor network. *Nature* **447**: 1130–1134.

Hermeking H. (2007). p53 enters the microRNA world. *Cancer Cell* **12**: 414–418.

Hillegass JM, Shukla A, Lathrop SA, MacPherson MB, Beuschel SL, Butnor KJ *et al*. (2010). Inflammation precedes the development of human malignant mesotheliomas in a SCID mouse xenograft model. *Ann N Y Acad Sci* **1203**: 7–14.

Huang C, Jiang T, Zhu L, Liu J, Cao J, Huang KJ *et al*. (2011a). STAT3-targeting RNA interference inhibits pancreatic cancer angiogenesis *in vitro* and *in vivo*. *Int J Oncol* **38**: 1637–1644.

Huang C, Yang G, Jiang T, Zhu G, Li H, Qiu Z. (2011b). The effects and mechanisms of blockage of STAT3 signaling pathway on IL-6 inducing EMT in human pancreatic cancer cells *in vitro*. *Neoplasma* **58**: 396–405.

Kim C, Kim DG, Park SH, Hwang YI, Jang SH, Kim CH *et al*. (2011). Epithelial to mesenchymal transition of mesothelial cells in tuberculous pleurisy. *Yonsei Med J* **52**: 51–58.

Kryczek I, Liu S, Roh M, Vatan L, Szeliga W, Wei S *et al*. (2011). Expression of aldehyde dehydrogenase and CD133 defines ovarian cancer stem cells. *Int J Cancer*.

Kubo T, Toyooka S, Tsukuda K, Sakaguchi M, Fukazawa T, Soh J *et al*. (2011). Epigenetic silencing of microRNA-34b/c lays an important role in the pathogenesis of malignant pleural mesothelioma. *Clin Cancer Res* **17**: 4965–4974.

Laberge RM, Awad P, Campisi J, Desprez PY. (2011). Epithelial-mesenchymal transition induced by senescent fibroblasts. *Cancer Microenviron*.

Li Q, Yano S, Ogino H, Wang W, Uehara H, Nishioka Y *et al*. (2007). The therapeutic efficacy of anti vascular endothelial growth factor antibody, bevacizumab, and pemetrexed against orthotopically implanted human pleural mesothelioma cells in severe combined immunodeficient mice. *Clin Cancer Res* **13**: 5918–5925.

Liu S, Ginestier C, Ou SJ, Clouthier SG, Patel SH, Monville F *et al*. (2011). Breast cancer stem cells are regulated by mesenchymal stem cells through cytokine networks. *Cancer Res* **71**: 614–624.

Ma I, Allan AL. (2011). The role of human aldehyde dehydrogenase in normal and cancer stem cells. *Stem Cell Rev* **7**: 292–306.

Marcato P, Dean CA, Pan D, Araslanova R, Gillis M, Joshi M *et al*. (2011). Aldehyde dehydrogenase activity of breast cancer stem cells

is primarily due to isoform ALDH1A3 and its expression is predictive of metastasis. *Stem Cells* **29**: 32–45.

Metcalf RA, Welsh JA, Bennett WP, Seddon MB, Lehman TA, Pelin K *et al*. (1992). p53 and Kirsten-ras mutations in human mesothelioma cell lines. *Cancer Res* **52**: 2610–2615.

Mor O, Yaron P, Huszar M, Yellin A, Jakobovitz O, Brok-Simoni F *et al*. (1997). Absence of p53 mutations in malignant mesotheliomas. *Am J Respir Cell Mol Biol* **16**: 9–13.

Mujoomdar AA, Tilleman TR, Richards WG, Bueno R, Sugarbaker DJ. (2010). Prevalence of in vitro chemotherapeutic drug resistance in primary malignant pleural mesothelioma: Result in a cohort of 203 resection specimens. *J Thorac Cardiovasc Surg* **140**: 352–355.

Oka M, Sakaguchi M, Okada T, Nagai H, Ozaki M, Yoshioka T *et al*. (2010). Signal transducer and activator of transcription 3 upregulates interleukin-8 expression at the level of transcription in human melanoma cells. *Exp Dermatol* **19**: e50–e55.

Park JS, Kim YS, Jee YK, Myong NH, Lee KY. (2003). Interleukin-8 production in tuberculous pleurisy: role of mesothelial cells stimulated by cytokine network involving tumour necrosis factor-alpha and interleukin-1 beta. *Scand J Immunol* **57**: 463–469.

Pompeo E, Albonici L, Doldo E, Orlandi A, Manzari V, Modesti A *et al*. (2009). Placenta growth factor expression has prognostic value in malignant pleural mesothelioma. *Ann Thorac Surg* **88**: 426–431.

Rodier F, Kim SH, Nijjar T, Yaswen P, Campisi J. (2005). Cancer and aging: the importance of telomeres in genome maintenance. *Int J Biochem Cell Biol* **37**: 977–990.

Ruco LP, de Laat PA, Matteucci C, Bernasconi S, Sciacca FM, van der Kwast TH *et al*. (1996). Expression of ICAM-1 and VCAM-1 in human malignant mesothelioma. *J Pathol* **179**: 266–271.

Scarpa S, Giuffrida A, Palumbo C, Coletti A, Cerrito MG, Vasaturo F *et al*. (2002). Retinoic acid inhibits fibronectin and laminin synthesis and cell migration of human pleural mesothelioma *in vitro*. *Oncol Rep* **9**: 205–209.

Schindler C, Levy DE, Decker T. (2007). JAK-STAT signaling: from interferons to cytokines. *J Biol Chem* **282**: 20059–20063.

Schramm A, Opitz I, Thies S, Seifert B, Moch H, Weder W *et al*. (2010). Prognostic significance of epithelial-mesenchymal transition in malignant pleural mesothelioma. *Eur J Cardiothorac Surg* **37**: 566–572.

Sidi R, Pasello G, Opitz I, Soltermann A, Tutic M, Rehrauer H *et al*. (2011). Induction of senescence markers after neo-adjuvant chemotherapy of malignant pleural mesothelioma and association with clinical outcome: an exploratory analysis. *Eur J Cancer* **47**: 326–332.

Sivertsen S, Hadar R, Elloul S, Vintman L, Bedrossian C, Reich R *et al*. (2006). Expression of Snail, Slug and Sip1 in malignant mesothelioma effusions is associated with matrix metalloproteinase, but not with cadherin expression. *Lung Cancer* **54**: 309–317.

Suzuki Y, Sakai K, Ueki J, Xu Q, Nakamura T, Shimada H *et al*. (2010). Inhibition of Met/HGF receptor and angiogenesis by NK4 leads to suppression of tumor growth and migration in malignant pleural mesothelioma. *Int J Cancer* **127**: 1948–1957.

Takeda K, Akira S. (2000). STAT family of transcription factors in cytokine-mediated biological responses. *Cytokine Growth Factor Rev* **11**: 199–207.

Tolnay E, Kuhnen C, Wiethege T, Konig JE, Voss B, Muller KM. (1998). Hepatocyte growth factor/scatter factor and its receptor c-Met are overexpressed and associated with an increased microvessel density in malignant pleural mesothelioma. *J Cancer Res Clin Oncol* **124**: 291–296.

Wang L, Park P, Zhang H, La Marca F, Lin CY. (2011). Prospective identification of tumorigenic osteosarcoma cancer stem cells in OS99-1 cells based on high aldehyde dehydrogenase activity. *Int J Cancer* **128**: 294–303.

Yao J, Wu X, Zhuang G, Kasman IM, Vogt T, Phan V *et al*. (2011). Expression of a functional VEGFR-1 in tumor cells is a major determinant of anti-PlGF antibodies efficacy. *Proc Natl Acad Sci USA* **108**: 11590–11595.

Young AR, Narita M. (2009). SASP reflects senescence. *EMBO Rep* **10**: 228–230.

Supplementary Information accompanies the paper on the Oncogene website (http://www.nature.com/onc)